



# Synthesis of zeolitic imidazolate framework-67 nanocube wrapped by graphene oxide and its application for supercapacitors

Wenjie Cao<sup>1</sup> · Miaomiao Han<sup>1</sup> · Lin Qin<sup>1</sup> · Qikang Jiang<sup>1</sup> · Junhui Xu<sup>1</sup> · Zhen Lu<sup>1</sup> · Yazhen Wang<sup>1</sup>

Received: 29 August 2018 / Revised: 11 October 2018 / Accepted: 26 October 2018 / Published online: 1 November 2018  
© Springer-Verlag GmbH Germany, part of Springer Nature 2018

## Abstract

In this study, a nanocube of zeolitic imidazolate framework-67 (ZIF-67) was prepared by blending cobalt nitrate hexahydrate and 2-methylimidazole together in aqueous solutions containing hexadecyltrimethylammonium bromide (CTAB). Then, graphene oxide (GO) wrapped ZIF-67 nanocomposites (ZIF-67/GO-*n*) were prepared by one-pot stirring method at room temperature. The morphology and microstructure of ZIF-67 and its GO nanocomposites were investigated by Raman spectra, X-ray diffraction (XRD), scanning electron microscopy (SEM), and Brunauer-Emmett-Teller (BET) specific surface area analysis. Electrochemical capacitance properties of all samples were characterized by cyclic voltammetry and chronopotentiometry, respectively. The results demonstrated that the content of GO used during synthesis process affected the specific capacity of nanocomposites while they were constructed as supercapacitor electrode. Compared with pure GO and ZIF-67 nanocubes, ZIF-67/GO-*n* composites had better specific capacitance. While the concentration of GO was 2 wt% based on their initial total mass of two reactants, ZIF-67/GO-2 composite presents a specific capacitance of 100.41 F g<sup>-1</sup> at a sweep rate of 5 mV s<sup>-1</sup>. The good electrochemical performance of ZIF-67/GO-*n* composite may be credited to large BET surface area of ZIF-67 nanocubes and good conductivity of GO, and thus is expected to become a potential electrode material for supercapacitors.

**Keywords** ZIF-67 · Graphene oxide · Composite · Electrode materials · Supercapacitor

## Introduction

It is of high important to exploit renewable energy sources and sustainable storage technologies because of the fast depletion of fossil fuels and the associated environmental pollution resulting from the burning. Supercapacitors (SCs), as one of the promising energy storage devices, have attracted considerable focus thanks to their outstanding features, such as high power density, ultrafast charge/discharge rate, good cycle stability, and environmental friendly [1, 2]. According to the electrochemical storage

mechanisms, SCs can be divided into electrical-double-layer capacitors (EDLCs) and pseudo-capacitors [3, 4]. EDLCs usually use carbon materials with high surface and good electric conductivity to store energy by electrostatic accumulation at the interface of carbon material on substrate and electrolyte. Pseudo-capacitors exploit near-surface oxidation-reduction of electrochemically active materials such as transition metal oxide [5, 6], conductive polymers [7, 8], and metal coordination compounds [9, 10]. Ordinarily, EDLCs can provide long cycle life, high charge/discharge rate, but low capacitance, while pseudo-capacitors possess high capacity, enhanced energy density but relatively poor circling life and rate performance [11, 12]. SCs have exhibited important application value in electric vehicles, backup power storage, aerospace systems, etc. [13, 14], of which the performance is chiefly depended on the electrode materials. Therefore, how to develop high performance electrode materials has and will become the focus of study in the field of SCs [15, 16].

Metal organic frameworks (MOFs), synthesized via the interconnection of metal ion nodes and organic linkers in suitable solvent, have attracted intense interest during the past

---

The first two authors contributed equally to this work and should be considered co-first authors.

✉ Yazhen Wang  
yazhenwang@163.com

<sup>1</sup> Key Laboratory of Optoelectronic Chemical Materials and Devices of Ministry of Education, Hubei Key Laboratory of Industrial Fume & Dust Pollution Control, School of Chemistry and Environmental Engineering, Jiangnan University, Wuhan 430056, Hubei, People's Republic of China

10 years owing to their high porosity, high surface area, and a tunable chemical property [17, 18]. With these versatile properties, MOFs have been extensively studied for gas storage and separation [19], sensors [17], catalysis [20], drug delivery [21], and energy storage and conversion [22–24]. In principle, the oxidation-reduction of metal ions provide an electronic channel, while the linker facilitate charge transfer in the framework [25]. However, most MOFs or MOF-derived materials exhibit poor conductivity and bad cycling stability in the process of charge/discharge, which restricts their application in SCs [26]. The introduction of some conductive materials such as carbon nano-tubes and graphene [10, 24, 27] improves the electrochemical performance of composites.

In this work, zeolitic imidazolate framework (ZIF-67) nanocubes, a subclass of MOFs, were easily synthesized by assembling cobalt ions and 2-methylimidazole ligands in the presence of surfactant hexadecyltrimethylammonium bromide (CTAB). Subsequently, graphene oxide (GO)-wrapped ZIF-67 nanocomposites (ZIF-67/GO) were synthesized by one-step stirring method at room temperature. The properties of synthesized materials were studied by Raman, XRD, SEM, and BET. When synthesized materials were utilized as electrodes for SCs, ZIF-67/GO nanocomposites exhibit enhanced specific capacitance and high cycling stability compared to single ZIF-67 and single GO. The test results show that the addition of a certain amount of GO can greatly improve the electrochemical performance of ZIF-67/GO composites as electrodes for SCs. Here, in comparison with the previous similar works in the literature, the uniform size and regular shape of ZIF-67 nanocubes wrapped by GO sheets was prepared by a simple method at room temperature in our work, which provide a new choice as the electrode material for supercapacitors.

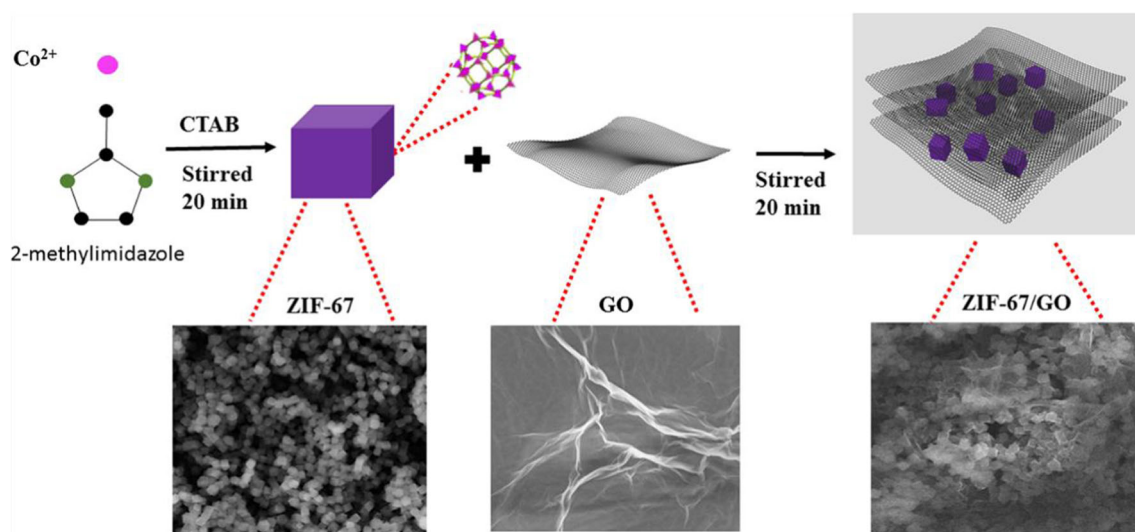
## Materials and methods

### Preparation of graphene oxide

Graphene oxide was prepared according to the Hummer's method [28] with modification. Briefly, 2.0 g graphite (Aladdin, 99.99%) and 1.0 g sodium nitrate (Sinopharm, analytical grade) were mixed into 46 ml sulfuric acid (Sinopharm, analytical grade) at 0 °C of ice-water bath with mechanical agitation for 10 min. After adding 6.0 g potassium permanganate (Sinopharm, analytical grade) into the above solution, the mixture was kept stirring for 30 min at 35 °C. Then, 100 ml redistilled water was added little by little until the temperature was up to 98 °C and kept for 20 min. Finally, the mixed solution including 260 ml redistilled water and 20 ml hydrogen peroxide (Sinopharm, 30%) was added at 98 °C for 20 min. The oxidized solution was washed using 5% hydrochloric acid and redistilled water several times. The yellow brown GO was obtained with centrifugation of 10,000 rpm for 10 min. After freeze-drying for 3 days, the GO powder was obtained.

### Preparation of ZIF-67 nanocubes

The nanocubes of ZIF-67 were easily obtained when mixing cobalt nitrate hexahydrate (Sinopharm, analytical grade) and 2-methylimidazole (Aladdin, 99%) in aqueous solutions including CTAB (Sinopharm, ≥ 99%), as described in the previous report [29]. First, 58 mg cobalt nitrate hexahydrate was dissolved in 2 ml redistilled water containing 1 mg of CTAB; 908 mg 2-methylimidazole was dissolved in 14 ml redistilled water. Then, mixing these two solutions and then vigorously stirring them at an ambient temperature, the purple



**Scheme 1** Schematic illustration of the synthesis process of GO wrapped ZIF-67 nanocubes (ZIF-67/GO composite)

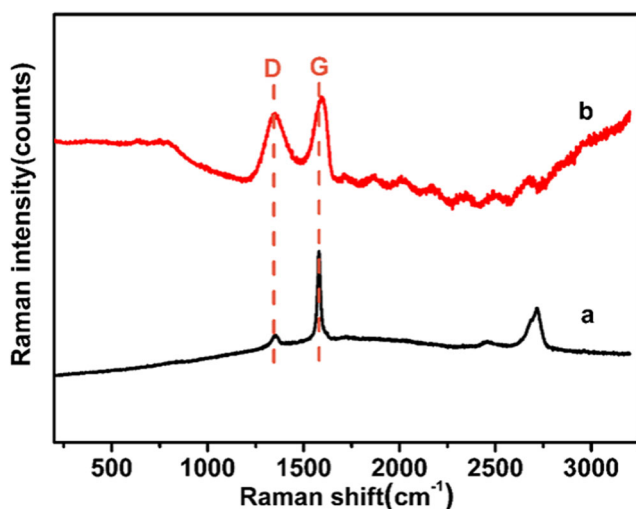


Fig. 1 Raman spectra of graphite (a) and graphene oxide (b)

precipitates were collected by centrifuging (10,000 rpm, 10 min) and followed by washing at least three times with water and methanol respectively. Finally, ZIF-67 nanocubes were dried at 80 °C for 4 h for ready to use.

### In situ preparation of ZIF-67/GO-*n* composites

The synthesis route of ZIF-67/GO-*n* composites is similar to that of ZIF-67 nanocubes. Before the fabrication of ZIF-67/GO, a certain concentration of GO aqueous suspension was first prepared with the assistance of ultrasonication. Then, the GO suspension was added into the pre-mixed solution containing 58 mg cobalt nitrate hexahydrate, 908 mg 2-methylimidazole, and 1 mg CTAB, and rapidly agitated for 20 min at room temperature. The final black products were labeled as ZIF-67/GO-*n*, where *n* = 1, 2, and 3 represent 1 wt%, 2 wt%, and 3 wt% GO added based on their initial total mass of Co(NO<sub>3</sub>)<sub>2</sub>·6H<sub>2</sub>O and 2-methylimidazole during the synthesis process, indicated as GO-1, GO-2, and GO-3. The in situ synthesis process of ZIF-67/GO composites was schematically illustrated in Scheme 1.

### Material characterization

The morphology of prepared materials was investigated by field emission scanning electron microscopy (FE-SEM, SU8000, Hitachi, Japan) with an operating voltage of 10.0 kV. The crystal structures of these materials were determined with an X-ray diffractometer (XRD, X'pert powder PANalytical, Netherlands) with Cu K<sub>α</sub> radiation ( $\lambda = 1.5410$  nm) over the  $2\theta$  range of 5–90° at 40 kV, 40 mA. N<sub>2</sub> adsorption-desorption isotherms were recorded with a surface area and porosity analyzer (Micromeritics 2020, ASAP, USA) at the temperature of liquid nitrogen (−196 °C). The

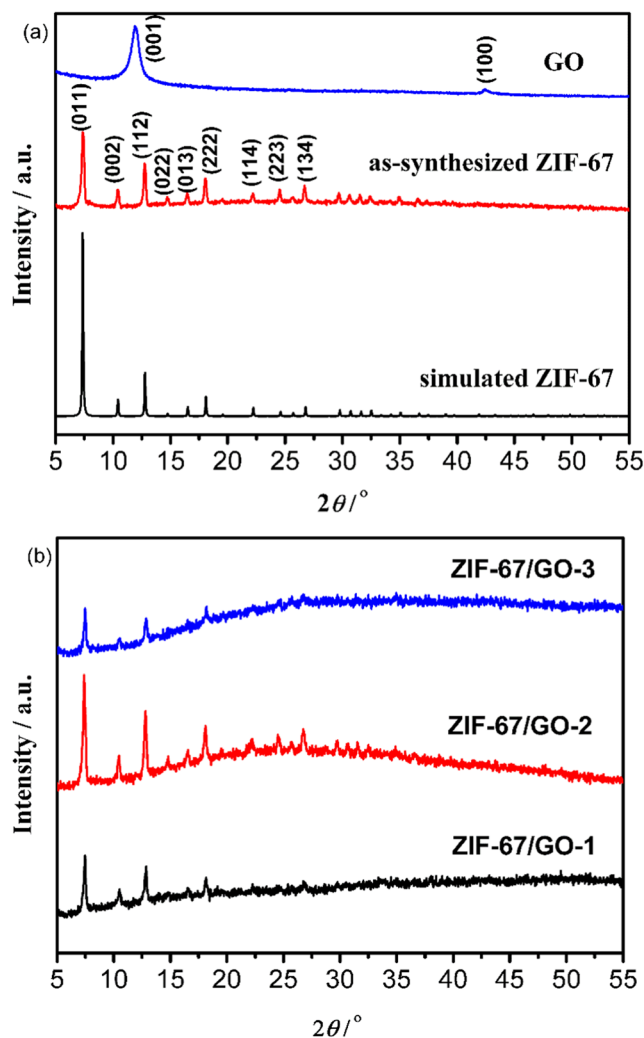


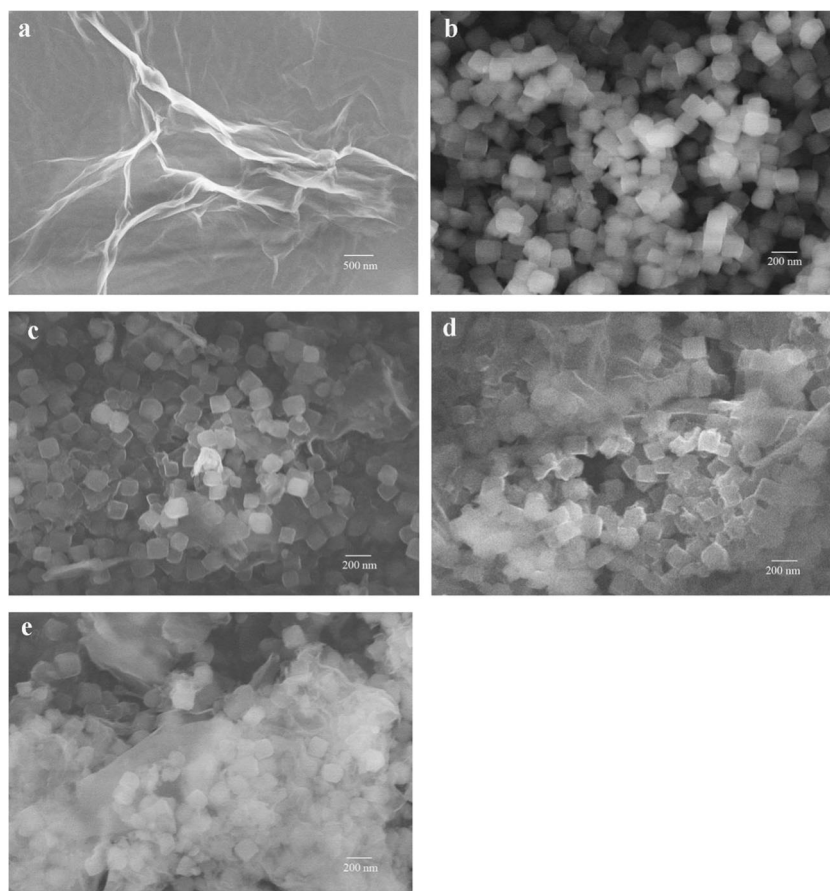
Fig. 2 **a** XRD patterns of GO, ZIF-67 nanocubes, and the simulated ZIF-67; **b** XRD patterns of ZIF-67/GO-*n* composite with different concentrations of GO

Brunauer-Emmett-Teller (BET) surface areas of ZIF-67 and ZIF-67/GO-2 was calculated based on the relative pressure ( $P/P_0$ ) values of 0.03–0.30, and yet the total pore volume was obtained at the  $P/P_0$  value to be 0.995. Raman spectra was carried out using a 532-nm laser with a Raman spectroscopy (Renishaw New Mills, UK) ranging from 100 to 3200 cm<sup>-1</sup>.

### Fabrication of supercapacitor electrodes

The above synthesized active materials, conductive carbon black power (CABOT, USA), and polyvinylidene fluoride (PVDF, HSV900, Arkema, France) were first mixed with a weight ratio of 8:1:1 in *N*-methyl-2-pyrrolidone (NMP, Aladdin, 99%,) to form slurry in agate mortar. The mass loading of active materials in this paper was on average 2.5 mg cm<sup>-2</sup>. Then, the slurry was carefully dipped into the

**Fig. 3** FE-SEM images of GO (a), ZIF-67 nanocubes (b), ZIF-67/GO-1 (c), ZIF-67/GO-2 (d), and ZIF-67/GO-3 (e)



clean nickel foam and the coated foam were dried for 4 h in a drying oven at 80 °C. Finally, the supercapacitor electrodes were pressed for 10 s under a pressure of 8 MPa for use.

## Electrochemical measurements

The electrochemical performance of all the supercapacitor electrodes was measured using CHI 660D electrochemical workstation (Shanghai Chenhua, China) in a three-electrode test system in 6 M KOH electrolyte solution. The supercapacitor electrode acted as the working electrode while Pt foil and saturated calomel electrode (SCE) as counter electrode and reference electrode. The cyclic voltammetry (CV) measurements were executed in the potential range of  $-0.3$ – $0.4$  V with different scan rates from 5 to 100  $\text{mV s}^{-1}$ , and the charge-discharge performance (GCD) was tested using chronopotentiometry technique by changing the current density in a potential window of  $-0.3$ – $0.35$  V. The voltammetric specific capacitance ( $C_s$  ( $\text{F g}^{-1}$ )) was derived from the integral area of CV curve by Eq. (1) [30]:

$$C_s = \frac{\int I dV}{2m\nu\Delta V} \quad (1)$$

where  $I$  (A) is the response current,  $m$  (g) is the mass of active material,  $\nu$  ( $\text{V s}^{-1}$ ) is the scan rate and  $\Delta V$  (V) is the absolute

value of the potential windows. The specific capacitance ( $C_s$  ( $\text{F g}^{-1}$ )) of GCD can also be determined through GCD curves according to Eq. (2) [31]:

$$C_s = \frac{It}{m\Delta V} = \frac{i_m t}{\Delta V} \quad (2)$$

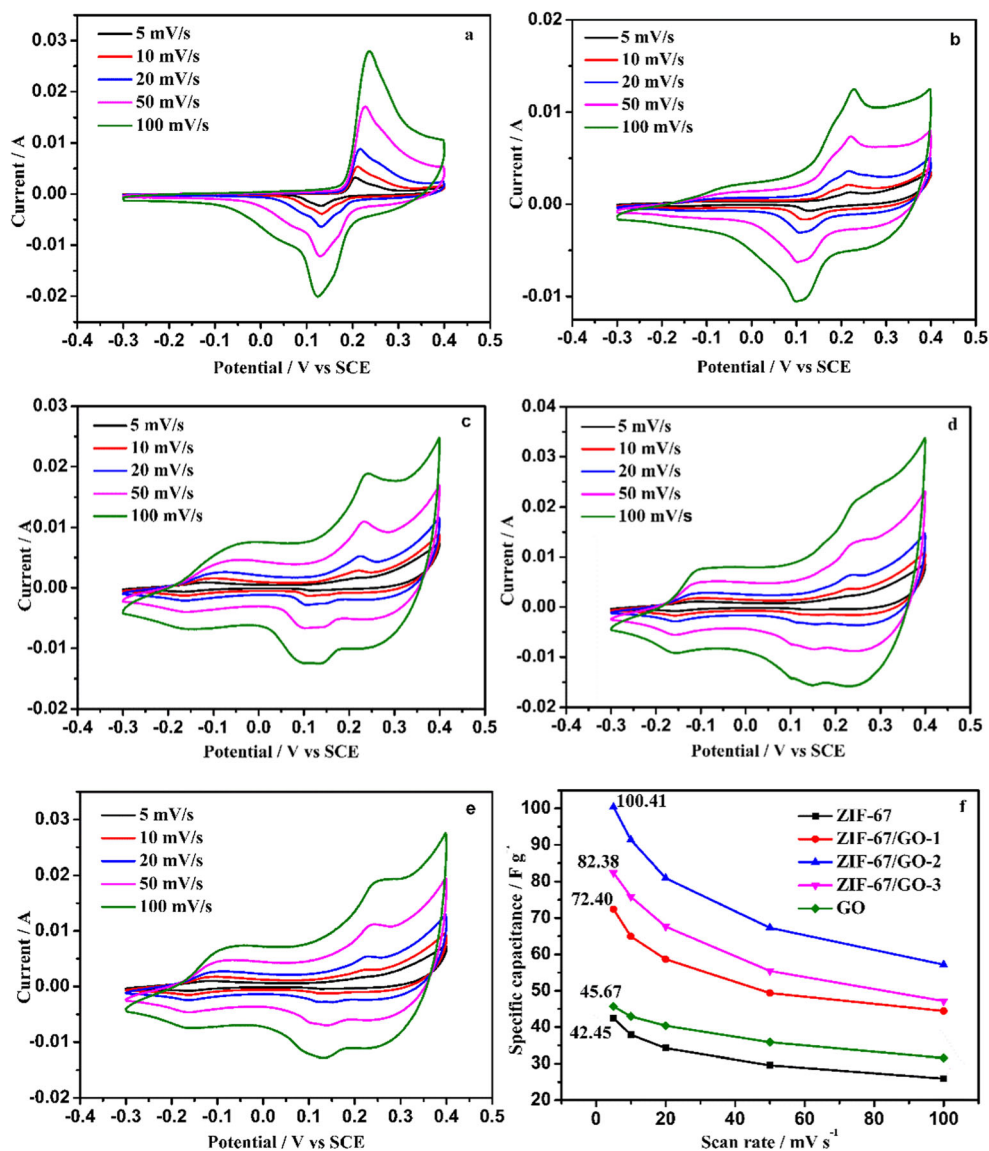
where  $i_m$  ( $\text{A g}^{-1}$ ) =  $I/m$  represents the discharge current density,  $t$  (s) represents the discharge time and  $\Delta V$  (V) represents the potential window applied in the process of discharge.

## Results and discussion

### Materials characterization

Raman spectroscopy is an extensively characterization tool for the study of carbon materials. As shown in Fig. 1, a strong sharp G band located at  $1581 \text{ cm}^{-1}$ , a small D band at  $1352 \text{ cm}^{-1}$ , and a 2D band at  $2716 \text{ cm}^{-1}$  were observed for graphite powder (curve a). Generally, the G band corresponds to  $\text{sp}^2$  carbon domains from the graphite lattice and the D band to defective/disordered graphitic carbon caused by the graphite edges [32, 33]. In the present graphite powder, the intensity of D band is relatively weak. However, the Raman spectrum of GO obtained by chemical treatment exhibits two intense G

**Fig. 4** Cyclic voltammetric curves of GO (a), ZIF-67 (b), ZIF-67/GO-1 (c), ZIF-67/GO-2 (d), ZIF-67/GO-3 (e) at different scan rates, and specific capacitances as a function of the scan rates for different electrodes (f)

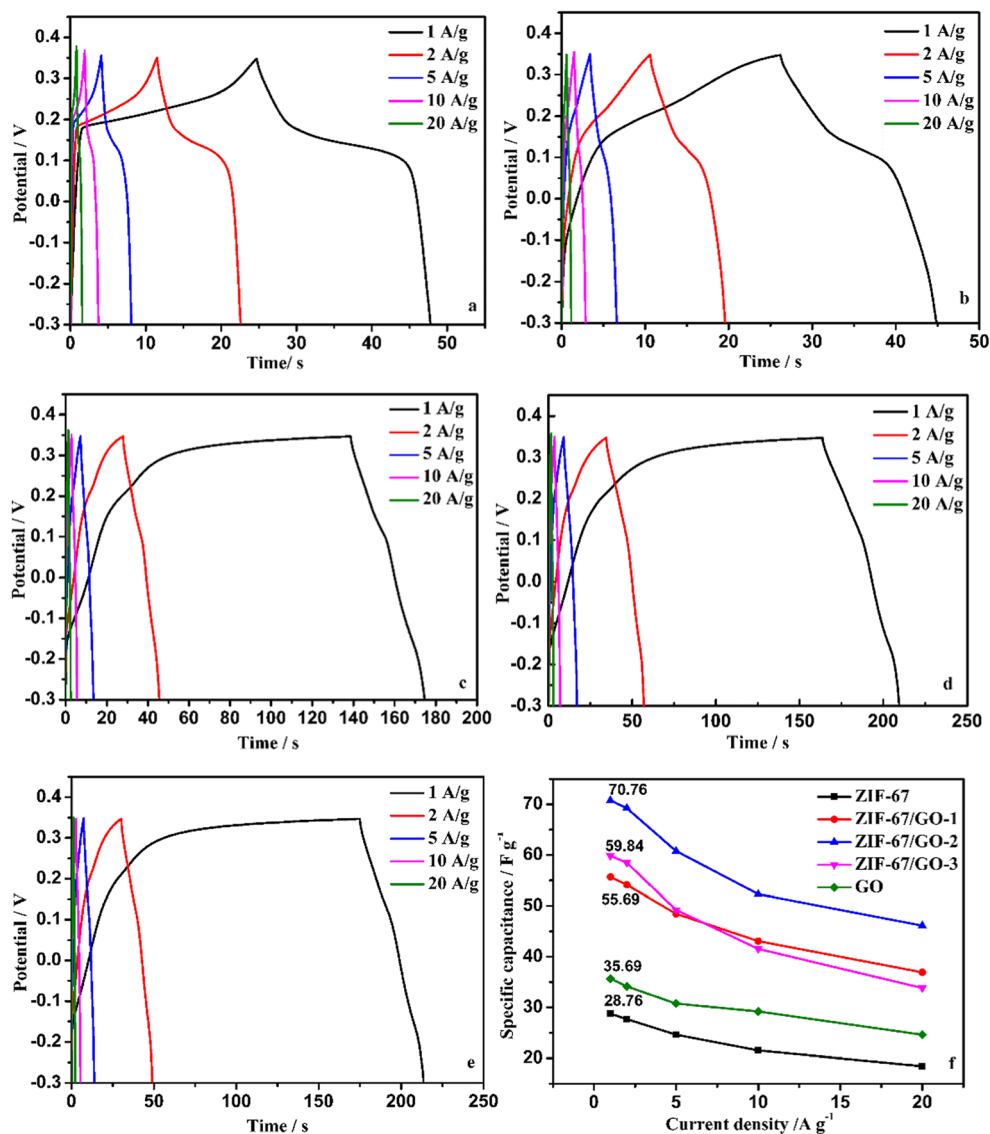


and D bands at  $1597\text{ cm}^{-1}$  and  $1355\text{ cm}^{-1}$ , respectively (curve b), which indicated that the G band appears some blue-shift for GO. Accordingly, the intensity of the D band enhances due to the existence of more  $\text{sp}^3$  domains or defects in GO [34]. In addition, these two bands are broadened compared to those of graphite. A universal account is that higher disorder in graphite results in a broader G band, as well as in a broader D band with relative higher intensity.

The crystallographic structure of the samples was analyzed using XRD, as displayed in Fig. 2. The XRD patterns of single GO, ZIF-67 nanocubes, and simulated ZIF-67 were given in Fig. 2a. In the GO pattern, the intense feature diffraction peak at  $2\theta = 11.9^\circ$  attributes to the crystal face of (001) with an interlayer spacing of 0.74 nm and the weak feature peak at  $2\theta = 42.5^\circ$  corresponds to the (100) crystal face, confirming the complete conversion of graphite into GO [35]. In comparison with the graphite interlayer spacing of ca. 0.34 nm [36],

the increase in interlayer spacing of GO can be ascribed to the incorporation of abundant oxygen-containing groups onto graphene layers during the oxidation process, which increased the disorder of structure [34]. The ZIF-67 nanocubes exhibit good crystal structure consisted with the reference [29]. The strong peaks of ZIF-67 nanocubes correspond to (011), (002), (112), (022), (013), (222), (114), (223), and (134) crystal faces, respectively, which coincide exactly with the simulated ZIF-67 pattern. Figure 2b shows the patterns of ZIF-67/GO-*n* composites with different GO concentrations. It was observed that the background signal of XRD patterns enhances slightly with the increasing amount of GO because of the amorphous phase of GO. All the composites show the similar patterns including four strong characteristic diffraction peak corresponding to (011), (002), (112), and (222) crystal faces of ZIF-67, indicating that the incorporation of GO did not destroy or disorganize the structure of ZIF-67 in composites

**Fig. 5** Chronopotentiometric curves of GO (a), ZIF-67 (b), ZIF-67/GO-1 (c), ZIF-67/GO-2 (d), ZIF-67/GO-3 (e) at different current densities, and specific capacitances as a function of the current density for different electrodes (f)



during in situ synthesis process. It was also found that the characteristic peaks of GO were not appeared in the patterns of ZIF-67/GO-*n* composites since the intensity of GO diffraction peak in comparison with that of ZIF-67 nanocubes are too weak to be detected by XRD, the result was consisted with the previous report [2].

The surface morphology of GO, ZIF-67, and ZIF-67/GO-*n* composites was investigated by FE-SEM in Fig. 3. The synthesized GO displays a typically lamellar and wrinkled morphology like a ruffled silk scarf (Fig. 3a). Figure 3b shows that the prepared ZIF-67 crystals have a uniform nanocubic shape with an average particle size of 150 nm, instead of the commonly obtained polyhedrons. The formation of nanocubic morphology was accredited to the addition of surfactants like CTAB, which can be adsorbed onto the hydrophobic surface of ZIF-67 crystals and then change the crystal growth rate [29, 37]. As shown in Fig. 3b–e, ZIF-67/GO-*n* composites exhibit a homogenous distribution of ZIF-67 which was still well-

maintained in shape after combining with GO in situ. Apparently, ZIF-67 nanocubes were wrapped in the GO sheets. The ZIF-67 nanocubes become more compact in a higher concentration of GO (Fig. 3e). From all these FE-SEM images, it can also be concluded that GO sheets were not only well assembled with ZIF-67 nanocubes, but also did not change the nanocubic structure of ZIF-67 in composites, which is consistent with the observation from XRD analysis.

### Electrochemical properties of supercapacitor electrodes

The electrochemical properties of single GO, single ZIF-67, and ZIF-67/GO-*n* composites investigated by CV curve and GCD curve are revealed in Figs. 4 and 5. Interestingly, the CV curves of GO give a pair of well-defined oxidation and reduction peaks at ca. 0.23 V and 0.13 V, respectively, as shown in Fig. 4a, indicating a pseudo-capacitive behavior of GO due to

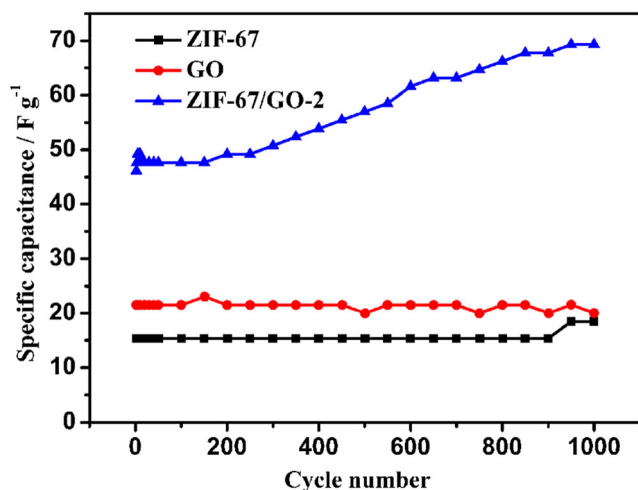


**Fig. 6** Capacitance cycle performance of GO (red line), ZIF-67 (black line), and ZIF-67/GO-2 (blue line) at the current density of  $10 \text{ A g}^{-1}$  in  $6 \text{ M KOH}$  electrolyte for 1000 cycles

the presence of abundant oxygen-containing functional groups. The similar result has been analyzed in the part of XRD analysis. The pseudo-capacitance of GO probably comes from electrochemical reactions between quinone/hydroquinone groups at the electrode interfaces [38–40]. However, two pairs of redox peaks were observed for all ZIF-67 and ZIF-67/GO-*n* composites in Fig. 4b–e. All these CV curves in shape clearly reveal that the capacitance characteristic of single ZIF-67 and ZIF-67/GO-*n* composites is also pseudo-capacitive behavior, which is well different from that of EDLCs associated with a relatively rectangular shape [41]. The capacitance of ZIF-67 and ZIF-67/GO-*n* composites might be largely attributed to the Faradaic reaction of Co(II)/Co(III) and Co(III)/Co(IV) redox couples inside the framework which was mediated by intercalation/deintercalation of

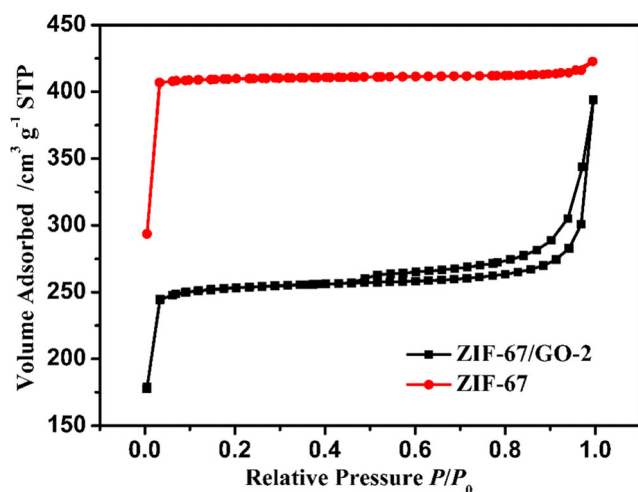


**Fig. 7**  $\text{N}_2$  adsorption-desorption isotherms of single ZIF-67 (black line) and ZIF-67/GO-2 composite (red line)

$\text{OH}^-$  ions from a alkali electrolyte solution on basis of the previous reports [42, 43]. Vitally, upon all these five active electrode materials, the shape of CVs and redox peaks potential almost remains unchanged with increasing scan rates and at the same time, the characteristic peak currents are linearly related with scan rates in the CV curves, suggesting that these electrodes have good reversibility and the redox reactions are belonged to the surface-controlled process, also a characteristics of pseudo-capacitive behavior.

Figure 4f shows the voltammetric specific capacitance values of different electrodes obtained from the integral area under the CV curves according to Eq. (1) at different scanning rates. It was observed that the specific capacitance of all materials decreases with the increase of scan rate due to limitation of ion diffusion rate. All the ZIF-67/GO-*n* composites present a higher specific capacitance in comparison with single GO and single ZIF-67 because of the synergetic effect between GO and ZIF-67. The ZIF-67/GO-2 composite exhibits the best CV specific capacitance of  $100.41 \text{ F g}^{-1}$  at the scanning rate of  $5 \text{ mV/s}$ , but the capacitance reduced to  $57.06 \text{ F g}^{-1}$  at the scanning rate of  $100 \text{ mV/s}$ . The test results proposed that charge transfer kinetics suffer higher restriction between electrodes and intercalation/deintercalation of  $\text{OH}^-$  at higher scan rate [10].

To further investigate the capacitive performance of different active electrode materials, the GCD tests were carried out with a potential range of  $-0.3$ – $0.35 \text{ V}$  at different current densities, as depicted in Fig. 5a–f. The shape of GCD curves also did not exhibit the characteristics of a pure EDLCs, but mostly pseudo-capacitive behavior, further demonstrating the capacitive characteristic of the materials in the CV analysis. All the GCD specific capacitances of ZIF-67/GO-*n* composites were higher than those of single GO and single ZIF-67 under the same condition, which is well agreeable with the results from the CV curves. The specific capacitance value derived from Eq. (2) vs. the discharge current density was constructed in Fig. 5f. The ZIF-67/GO-2 electrode also exhibited the best GCD specific capacitance at the same current density. The GCD specific capacitance of ZIF-67/GO-2 composite is up to  $70.76 \text{ F g}^{-1}$  at the lower current density of  $1 \text{ A g}^{-1}$  and  $46.36 \text{ F g}^{-1}$  at the higher current density of  $20 \text{ A g}^{-1}$ . This result may also be explicated by considering the  $\text{OH}^-$  ion diffusion rate during the charge-discharge processes. At higher current density, the unfavorable accessibility of  $\text{OH}^-$  ions in the interface of electrolyte solution and electrode cannot meet the demand [10, 44].

In addition, the specific capacitance values of ZIF-67/GO-*n* composites were influenced by the amount of GO added in the composite. Similar trends were observed in the CV and GCD performance. While the weight ratio of GO was 2% based on the initial total weight of two reactants during the synthesis of the composites, the best specific capacitance was obtained for ZIF-67/GO-2, which indicated that the ZIF-67/GO-2 composite can store more charge than the others. As mentioned in

**Table 1** Comparison of the porosity of ZIF-67 and ZIF-67/GO-2 composite

Parameters	ZIF-67	ZIF-67/GO-2
BET surface area	1222.15 m <sup>2</sup> g <sup>-1</sup>	763.06 m <sup>2</sup> g <sup>-1</sup>
Pore volume	0.65 cm <sup>3</sup> g <sup>-1</sup>	0.60 cm <sup>3</sup> g <sup>-1</sup>
Adsorption average pore width (4 V/A by BET)	2.13 nm	3.19 nm

SEM images, it can be included that ZIF-67 nanocubes were grown with GO in situ and synchronously well wrapped by GO nanosheets. The ZIF-67 nanocubes at a higher content of GO become more compact. The introduction of GO nanosheets can serve as electron/charge transfer carrier and bring more active sites of ZIF-67 for oxidation-reduction reactions due to its good conductivity. On the other hand, a high content GO may conceal some of the exposed active sites in the framework and prevent ZIF-67 from effectively contacting with electrolyte [2]. Hence, the specific capacitance of ZIF-67/GO-3 composite displays a certain reduction in comparison with that of ZIF-67/GO-2 composite.

The cycle life of single GO, single ZIF-67 nanocubes, and ZIF-67/GO-2 composite was measured by a chronopotentiometric technique at 10 A g<sup>-1</sup> in 6 M KOH solution. These supercapacitor electrodes displayed good cycle stability, as depicted in Fig. 6. The specific capacitance of GO kept 95.3% of its original value after 1000 cycles (red line). The capacitance of pure ZIF-67 almost retains a constant value during 900 cycles, but there is a slightly increase between 900 and 1000 cycles (black line). The eventual specific capacitance value of ZIF-67 was 118% of its original value. However, the cycling performance test of ZIF-67/GO-2 composite shows that the capacitance value increases to 62.06 Fg<sup>-1</sup> after 600 cycles and remained only a slight increase from 600 to 1000 cycles. The final capacitance value of ZIF-67/GO-2 composite was up to 150% of its original value after 1000 cycles (blue line). The increasing capacitance with the cycle charge-discharge process might be ascribed to activation of the ZIF-67/GO-2 composite with time, since it takes a certain time for electrolytes to permeate the interior of the electrode materials [45]. The similar result was reported in the previous reference [42].

### Nitrogen adsorption-desorption properties of ZIF-67 and ZIF-67/GO-2

Figure 7 depicted the N<sub>2</sub> adsorption-desorption isotherm of pure ZIF-67 and ZIF-67/GO-2 composite. The specific values associated with pore texture, such as BET surface areas and pore volume, are summarized in Table 1. Apparently, N<sub>2</sub> adsorption-desorption isotherms for ZIF-67 resembles a reversible type I isotherm (red line), suggesting a characteristics of microporous material. A sharp increase near Y-axis at low relative pressure for the isotherm of ZIF-67 also imply the presence of micropores.

The sudden increase at high relative pressure can be ascribed to physisorbed liquid nitrogen on the surface of the nanoparticles [46]. The ZIF-67 nanocubes with an average pore diameter of 2.13 nm has an extremely large BET surface of 1222.1 m<sup>2</sup> g<sup>-1</sup> and total volume of 0.654 cm<sup>3</sup> g<sup>-1</sup>. These values are higher than the values reported previously from ZIF-67 polyhedrons without adding surfactant [46, 47]. However, a characteristics small hysteresis loop at relative pressure between 0.48 and 0.98 is observed for the isotherm of ZIF-67/GO-2 composite, representing the type I of isotherms with a H4-type hysteresis loop. This behavior suggests the coexistence of mesopores from composite. The BET surface of 763.0 m<sup>2</sup> g<sup>-1</sup> and a micropore volume of 0.609 cm<sup>3</sup> g<sup>-1</sup> are also estimated for ZIF-67/GO-2 composite with an average pore diameter of 3.19 nm. Moreover, the decrease in BET surface of ZIF-67/GO-2 composite in comparison with ZIF-67 is due to the addition of GO where ZIF-67 nanocubes can be wrapped by the lamellar GO. The coexistence of mesopores from composite could play a key part in high specific capacitance of ZIF-67/GO-2 composite owing to favorable intercalation/deintercalation of OH<sup>-</sup> ions at the electrode [48]. The result here does match well with those discussed above.

### Conclusions

In summary, ZIF-67/GO-n composites with different concentrations of GO were synthesized by an in situ hydrothermal method at room temperature. Since ZIF-67 nanocubes can provide large BET surface of 1222.1 m<sup>2</sup> g<sup>-1</sup> compared to the commonly observed polyhedrons of ZIF-67, and GO have good electron conductivity, the specific capacitance values of ZIF-67/GO-n composites were significantly higher than those of single GO and single ZIF-67. The ZIF-67/GO-2 composite, which has 2 wt% GO based on the initial total weight of two reactants, showed the best CV capacitance of 100.41 F g<sup>-1</sup> at the low scan rate of 5 mV/s and the best GCD capacitance of 70.76 F g<sup>-1</sup> at the low current density of 1 A g<sup>-1</sup>. Both single ZIF-67 and ZIF-67/GO-2 composite also displayed good cycle performance. Owing to the addition of GO, electrolyte ions can favorably intercalate/deintercalate between electrolyte and ZIF-67 nanocubes wrapped by GO. Hence, the ZIF-67/GO composite can be developed as a latent electrode material for supercapacitors.

**Funding information** This work was financially supported by the Open Foundation of Key Laboratory of Optoelectronic Chemical Materials and Devices of Ministry of Education (No.JDGD-2016008), the Open Foundation of Hubei Key Laboratory of Industrial Fume & Dust Pollution Control (No.HBIK2016-01) and the National Training Programs of Innovation and Entrepreneurship for undergraduates (No.2017zd041).

## References

- Wang YG, Song YF, Xia YY (2016) Electrochemical capacitors: mechanism, materials, systems, characterization and applications. *Chem Soc Rev* 45(21):5925–5950
- Lv ZJ, Zhong Q, Bu YF (2018) In-situ conversion of rGO/Ni<sub>2</sub>P composite from GO/Ni-MOF precursor with enhanced electrochemical property. *Appl Surface Sci* 439:413–419
- Suominen M, Lehtimäki S, Yewale R, Damlin P, Tuukkanen S, Kvarnström C (2017) Electropolymerized polyazulene as active material in flexible supercapacitors. *J Power Sources* 356:181–190
- Jafari EA, Moradi M, Borhani S, Bigdeli H, Hajati S (2018) Fabrication of hybrid supercapacitor based on rod-like HKUST-1@polyaniline as cathode and reduced graphene oxide as anode. *Phys E Low-dimensional Sys Nanostructures* 99:16–23
- Raj CJ, Rajesh M, Manikandan R, Sim JY, Yu KH, Park SY, Song JH, Kim BC (2017) Two-dimensional planar supercapacitor based on zinc oxide/manganese oxide core/shell nano-architecture. *Electrochim Acta* 247:949–957
- Madhuvilakku R, Alagar S, Mariyappan R, Piraman S (2017) Green one-pot synthesis of flowers-like Fe<sub>3</sub>O<sub>4</sub>/rGO hybrid nanocomposites for effective electrochemical detection of Riboflavin and low-cost supercapacitor applications. *Sens Actuators B Chem* 253:879–892
- Htut KZ, Kim M, Lee E, Lee G, Baek SH, Shim SE (2017) Biodegradable polymermodified graphene/polyaniline electrodes for supercapacitors. *Synth Met* 227:61–70
- Hosseini MG, Shahryari E (2017) Fabrication of novel solid-state supercapacitor using a Nafion polymer membrane with graphene oxide/multiwalled carbon nanotube/polyaniline. *J Solid State Electrochem* 21(10):2833–2848
- Zhao Y, Song ZX, Li X, Sun Q, Cheng NC, Lawes S, Sun XL (2016) Metal organic frameworks for energy storage and conversion. *Energy Storage Mater* 2:35–62
- Zhou YJ, Mao M, Wang W, Yang ZK, Liu X (2016) In-Situ fabrication of graphene oxide hybrid Ni-based metal-organic framework (Ni-MOFs@GO) with ultrahigh capacitance as electrochemical pseudocapacitor materials. *ACS Appl Mater Interfaces* 8(42):28904–28916
- Wang L, Han YZ, Feng X, Zhou JW, Qi PF, Wang B (2016) Metal-organic frameworks for energy storage: batteries and supercapacitors, coordination. *Chem Rev* 307:361–381
- Qu C, Jiao Y, Zhao BT, Chen DC, Zou RQ, Walton KS, Liu ML (2016) Nickel-based pillared MOFs for high-performance supercapacitors: design, synthesis and stability study. *Nano Energy* 26:66–73
- Yu M, Lin D, Feng H, Zeng Y, Tong Y, Lu X (2017) Boosting the energy density of carbon-based aqueous supercapacitors by optimizing the surface charge. *Angew Chem Int Ed* 56(20):5454–5459
- Zeng Y, Lin Z, Meng Y, Wang Y, Yu M, Lu X, Tong Y (2016) Flexible ultrafast aqueous rechargeable Ni||Bi battery based on highly durable single-crystalline bismuth nanostructured anode. *Adv Mater* 28(41):9188–9195
- Wang G, Zhang L, Zhang J (2012) A review of electrode materials for electrochemical supercapacitors. *Chem Soc Rev* 41(2):797–828
- Gao T, Zhou F, Ma W, Li HB (2018) Metal-organic-framework derived carbon polyhedron and carbon nanotube hybrids as electrode for electrochemical supercapacitor and capacitive deionization. *Electrochim Acta* 263:85–93
- Haldorai Y, Choec SR, Huh YS, Han YK (2018) Metal-organic framework derived nanoporous carbon/Co<sub>3</sub>O<sub>4</sub> composite electrode as a sensing platform for the determination of glucose and high-performance supercapacitor. *Carbon* 127:366–373
- Slater MD, Kim D, Lee E, Johnson CS (2013) Sodium-ion batteries. *Adv Funct Mater* 23(8):947–958
- Kayal S, Sun B, Chakraborty A (2015) Study of metal-organic framework MIL-101(Cr) for natural gas (methane) storage and compare with other MOFs (metal-organic frameworks). *Energy* 91:772–781
- Huang YB, Liang J, Wang XS, Cao R (2017) Multifunctional metal-organic framework catalysts: synergistic catalysis and tandem reactions. *Chem Soc Rev* 46(1):126–157
- Zheng H, Zhang Y, Liu L, Wan W, Guo P, Nyström AM, Zou XD (2016) One-pot Synthesis of metal-organic frameworks with encapsulated target molecules and their applications for controlled drug delivery. *J Am Chem Soc* 138(3):962–968
- Choi KM, Jeong HM, Park JH, Zhang YB, Kang JK, Yaghi OM (2014) Supercapacitors of nanocrystalline metal-organic frameworks. *ACS Nano* 8(7):7451–7457
- Guo SN, Zhu Y, Yan YY, Min YL, Fan JC, Xu QJ, Yun H (2016) (Metal-Organic Framework)-Polyaniline sandwich structure composites as novel hybrid electrode materials for high-performance supercapacitor. *J Power Sources* 316:176–182
- Hong JY, Jung YJ, Park DW, Chung S, Kim S (2018) Synthesis and electrochemical analysis of electrode prepared from zeolitic imidazolate framework (ZIF)-67/graphene composite for lithium sulfur cells. *Electrochim Acta* 259:1021–1029
- Yang L, McNichols BW, Davidson M, Schweitzer B, Gómez-Gualdrón DA, Trewyn BG, Sellinger A, Carreon MA (2017) Noble metal-free catalytic decarboxylation of oleic acid to n-heptadecane on nickel-based metal-organic frameworks (MOFs). *Catal Sci Technol* 7(14):3027–3035
- Kang L, Sun SX, Kong LB, Lang JW, Luo YC (2014) Investigating metal-organic framework as a new pseudo-capacitive material for supercapacitors. *Chin Chem Lett* 25(6):957–961
- Wang P, Li CY, Wang WG, Wang J, Zhu YS, Wu YP (2018) Hollow Co<sub>9</sub>S<sub>8</sub> from metal organic framework supported on rGO as electrode material for highly stable supercapacitors. *Chin Chem Lett* 29(4):612–615
- Hummers WS Jr, Offeman RE (1958) Preparation of graphitic oxide. *J Am Chem Soc* 80(6):1339–1339
- Hu H, Guan BY, Lou XW(D) (2016) Construction of complex CoS hollow structures with enhanced electrochemical properties for hybrid supercapacitors. *Chem* 1(1):102–113
- Borhani S, Moradi M, Kiani MA, Hajati S, Toth J (2017) CoxZn1-x ZIF-derived binary Co<sub>3</sub>O<sub>4</sub>/ZnO wrapped by 3D reduced graphene oxide for asymmetric supercapacitor: comparison of pure and heat-treated bimetallic MOF. *Ceram Int* 43(16):14413–14425
- Hu B, Qin X, Asiri AM, Alamry KA, Youbi AI AO, Sun X (2013) Fabrication of Ni(OH)<sub>2</sub> nanoflakes array on Ni foam as a binder-free electrode material for high performance supercapacitors. *Electrochim Acta* 107:339–342
- Zhang C, Mahmood N, Yin H, Liu F, Hou Y (2013) Synthesis of phosphorus-doped graphene and its multifunctional applications for oxygen reduction reaction and Lithium ion batteries. *Adv Mater* 25(35):4932–4937
- Kudin KN, Ozbas B, Schniepp HC, Prud'homme RK, Aksay IA, Car R (2008) Raman spectra of graphite oxide and functionalized graphene sheets. *Nano Lett* 8(1):36–41

34. Silva De KKH, Huang HH, Joshi RK, Yoshimura M (2017) Chemical reduction of graphene oxide using green reductants. *Carbon* 119:190–199
35. Channei D, Nakaruk A, Phanichphant S (2017) Influence of graphene oxide on photocatalytic enhancement of cerium dioxide. *Mater Lett* 209:43–47
36. Krishnamoorthy K, Veerapandian M, Yun K, Kim SJ (2013) The chemical and structural analysis of graphene oxide with different degrees of oxidation. *Carbon* 53:38–49
37. Pan YC, Heryadi D, Zhou F, Zhao L, Lestari G, Su HB, Lai ZP (2011) Tuning the crystal morphology and size of zeolitic imidazolate framework-8 in aqueous solution by surfactants. *CrystEngComm* 13(23):6937–6940
38. Xu B, Yue SF, Sui ZY, Zhang XT, Hou SS, Cao GP, Yang YS (2011) What is the choice for supercapacitors: graphene or graphene oxide? *Energy Environ Sci* 4(8):2826–2830
39. Zhang X, Zhang DC, Chen Y, Sun XZ, Ma YW (2012) Electrochemical reduction of graphene oxide films: preparation, characterization and their electrochemical properties. *Chin Sci Bull* 57(23):3045–3050
40. Aboutalebi SH, Chidembo AT, Salari M, Konstantinov K, Wexler D, Liu HK, Dou SX (2011) Comparison of GO, GO/MWCNTs composite and MWCNTs as potential electrode materials for supercapacitors. *Energy Environ Sci* 4(5):1855–1865
41. El-Kady MF, Strong V, Dubin S, Kaner RB (2012) Laser scribing of high-performance and flexible graphene-based electrochemical capacitors. *Science* 335(6074):1326–1330
42. Zhang D, Shi H, Zhang R, Zhang Z, Wang N, Li J, Yuan B, Bai H, Zhang J (2015) Quick synthesis of zeolitic imidazolate framework microflowers with enhanced supercapacitor and electrocatalytic performances. *RSC Adv* 5(72):58772–58776
43. Meng W, Wen YY, Dai L, He ZX, Wang L (2018) A novel electrochemical sensor for glucose detection based on Ag@ZIF-67 nanocomposite. *Sens Actuators B Chem* 260:852–860
44. Kotz R, Carlen M (2000) Principles and applications of electrochemical capacitors. *Electrochim Acta* 452:2483–2498
45. Gao Y, Wu J, Zhang W, Tan Y, Gao J, Tang B, Zhao J (2014) Synthesis of nickel carbonate hydroxide/zeolitic imidazolate framework-8 as a supercapacitors electrode. *RSC Adv* 4(68):36366–36371
46. Diring S, Furukawa S, Takashima Y, Tsuruoka T, Kitagawa S (2010) Controlled multiscale synthesis of porous coordination polymer in nano/micro regimes. *Chem Mater* 22(16):4531–4538
47. Gross AF, Sherman E, Vajo JJ (2012) Aqueous room temperature synthesis of cobalt and zinc sodalite zeolitic imidizolate frameworks. *Dalton Trans* 41(18):5458–5460
48. Srimuk P, Luanwuthi S, Krittayavathananon A, Sawangphruk M (2015) Solid-type supercapacitor of reduced graphene oxide-metal organic framework composite coated on carbon fiber paper. *Electrochim Acta* 157:69–77